Multifunctional A356 Aluminum Composites Reinforced with CeO_2, MoS_2, and Ni via Friction Stir Processing for Automotive and Electrical Applications

L. Gyansah[1*], J. K. Annan[2]

[1]Assemblies of God, Institute of Higher Learning, Krunum-Afrancho, Ghana

[2]University of Mines and Technology, Tarkwa, Ghana

***Corresponding Author**

DOI: https://doi.org/10.51584/IJRIAS.2025.10120009

Received: 16 December 2025; Accepted: 24 December 2025; Published: 01 January 2026

ABSTRACT

This research paper incorporated and explored the different physical and chemical properties of three reinforcement materials-5 wt. % CeO_2, 5 wt. % MoS_2, and 3 wt. % Ni particles in aluminum composites processed by Friction Stir Processing (FSP) in multiple property domains for applications in automobile, electrical and electronic industries. The severe plastic deformation and dynamic recrystallization during FSP process led to significant grain refinement of the aluminum matrix and uniform-dispersion of the CeO_2 and MoS_2, which resulted in a refined grain structure and grain boundary strengthening. The dispersed ceramic particles and Ni particles act as nucleation sites for new grains during FSP process and pin grain boundaries, thereby restricting grain growth. This led to a finer, more homogeneous microstructure in the stir zone. Grains per square inch when examined through a 500 X magnification was determined to be 1520. The interfacial bonding layers between the matrix A356 and reinforcements CeO_2, MoS_2, and Ni fabricated using the FSP method revealed dendritic feature-like layers with robust and cohesive bond strength. Moreover, XRD revealed no formation of new intermetallic phases which confirmed an excellent processed composite. The refined grain structure (i.e. Hall-Petch effect) further contributes to the enhanced hardness (61.32 %), wear (56.8 %) and tensile strength (35 %) of the composite. The implantation of the particles contributed to lower wear rates and improved wear resistance. Corrosion resistance, performed in a 3.5 wt. % NaCl solution for 120 hours, revealed enhanced protection in aggressive environments pertaining to the development of protective oxide-layers by CeO_2 and MoS_2. Incorporation of 3 wt.% Ni substantially improved electrical performance and multi-pass FSP improved the metallic network, increasing conductivity by 10-15 % relative to the single-pass composite. Contact resistance on the other hand remained within the range required for low-current conduction, electronic housings, and heat-spreader applications, though still higher than base A356. These analyses underscored the multifaceted benefits of incorporating 5 wt. % CeO_2, 5 wt. % MoS_2, and 3 wt. % Ni particles in A356 composites fabricated through FSP method.

Keywords: Bonding Mechanism, Electrical Properties, Friction Stir Processing, Ceramic Particles, Nickel, Corrosion, Contact Resistance, Wear, Mechanical Testing

INTRODUCTION

Reinforcing hard ceramic particles in aluminum composite materials offers a lot of advantages and applications. Incorporating ceramic particles serve as reinforcement, vitally enhancing the mechanical strength of the composite [1]. These include improved hardness, tensile strength and flexural strength for structural application purposes [2, 3]. Ceramics exhibit excellent thermal properties, making the composite to offer resistance to high temperatures without structural degradation. This makes it applicable to aerospace and automotive industries [4]. Ceramics particles can improve the composite's corrosion resistance and extend its service life in corrosive environments. Despite the addition of ceramics, these composites remain relatively lightweight making them suitable for weight-sensitive industries like aerospace [5].

Aluminum-based composites (AMCs) have attracted vital attention in many industries pertaining to their

unique-combination of improved electrical characteristics, mechanical, thermal and lightweight properties [6, 7]. These composites consist of aluminum material as the matrix and ceramic phases as reinforcement, which trigger enhanced performance attributes. AMCs application is normally utilized in the aerospace industry due to their lightweight nature which reduces the overall weight of aircraft and space shuttle, enhancing fuel efficiency and payload capacity[8]. Imperatively, AMCs withstands structural components and improves heat-resisting shields [9]. Automotive sector used AMC to reduce vehicle weight amid better fuel efficiency and reduction in emissions [10]. These composites are applied in body panels, engine components and chassis systems. Prominently, AMC are used in electronics industry to fabricate substrates for printed circuit boards (PCBs) pertaining to their excellent thermal conductivity and reliable performance [11]. Moreover, AMC are utilized in the construction of sports equipment, marine vessels, and industrial machinery due to its lightweight, durability, and corrosion-resistant characteristics.

Friction Stir Processing (FSP) is a unique technique for the manufacturing of advanced AMCs [12]. FSP utilizes a high-strength rotating-tool that is positioned on the surface of an aluminum substrate, producing a solid-state bond between the aluminum matrixes and reinforcing materials. FSP enhances a uniformly-dispersion of reinforcement materials within the aluminum matrixes [13]. This results in a refined microstructure with refined grain size and enhances mechanical properties. FSP improves the hardness, mechanical strength and toughness of AMCs, potential for industrial applications. FSP bonding mechanism as a solid-state reduces interfacial defects normally found in conventional fusion-based processes [14]. The technique allows for precise control for tailoring composite's microstructure to improve properties by varying processing parameters dub feed rate, tool rotation speed and tool design [15]. Furthermore, FSP eliminates issues associated with the heat-affected zone (HAZ) normally observed in fusion welding methods, thereby improving corrosion resistance and metallurgical defects [16].

Although research has been ongoing on AMCs fabricated by FSP method, the specific effects of CeO_2-MoS_2-Ni particles reinforced in aluminum matrix-composites are still in the neonate stage. Some researchers studied the influence of single reinforcement material AMCs, there are no combined incorporation of CeO_2, MoS_2, and Ni in the FSP-processed AMCs. Moreover, other researchers primarily focused on a single reinforcement to extract its mechanical properties or corrosion resistance. Those studies did not consider the holistic characterization of the microstructure evolution, bonding mechanisms, wear resistance and corrosion performance. Hence, this paper will address these scientific gaps.

By combining CeO_2, MoS_2, and Ni as reinforcement materials, this research explores the combine effects of these elements within AMCs using FSP method. The intent of this research is to address the current dearth of knowledge and provide significant contributions into the development of high-performance AMCs with potential applications in automobile, electrical and electronic Industries. The findings of this paper have the potential to advance the design and engineering of Al-based composites for a broad-array of prominent applications.

MATERIALS AND METHODS

Aluminum alloy A356 was employed with chemical composition: Al-6.5Si-0.6Fe-0.45Mg obtained from Angang Group Aluminium Powder Co., Ltd, China. X-Ray Diffraction (XRD) technique was used to probe the chemical composition of the A356 alloy. The superior lightweight, heat-treatability and high mechanical strength were unique characteristics of this alloy. The material demonstrates a tensile-strength of about 310 MPa. An alloy made from A356 has a hardness of 58.6 HV [17].

The powder size distributions were measured with (Mastersizer 2000, Malvern Instruments Ltd, UK).Three different reinforcement particles were used for this test (i.e. Ceria or cerium dioxide (CeO_2), Molybdenum disulfide (MoS_2) and Nickel (Ni)). The Ceria powder size has surface weighted mean of 16.56 μm and volume weighted mean of 20.45 μm with medium size d50=18.62μm). The MoS_2 powder on the other hand, has surface weighted mean 11.305 μm) and volume weighted mean (12.53 μm) with medium size (d50=11.92 μm). The Ni powder has weighted mean of 15.46 μm and volume weighted mean of 17.66 μm with medium size d50=16.73).

CeO_2 is an oxide that possesses remarkable characteristics pertaining to its significant oxygen storage capacity.

ISSN No. 2454-6194 | DOI: 10.51584/IJRIAS |Volume X Issue XII December 2025

It is used in automobile catalytic-converters and possesses good thermal stability and electrical conductivity especially when combined with conductive Ni particles and semiconducting MoS_2 [18, 19]. In SEM images (Figure 1 (a)), CeO_2 powder particles typically displayed a variety of morphologies, including spherical, agglomerated, or irregular shapes.

Molybdenum disulfide (MoS_2) is a layered transition-metal dichalcogenide. It has unique properties such as electrical conductivity, high lubricity and thermal stability [20, 21]. MoS_2 is utilized as a solid lubricant mainly in semiconductor devices and for energy storage systems. In SEM images (Figure 1 (b)), MoS_2 powder particles often exhibit distinct platelet-like or layered structures pertaining to its crystalline nature. These particles tend to stack together in thin layers, which result in a high surface area-to-volume ratio. Their morphology is suitable for various applications in lubricants and catalysts. Furthermore, MoS_2 particles can agglomerate affecting their uniform dispersion and properties depending on the synthesis method and processing conditions.

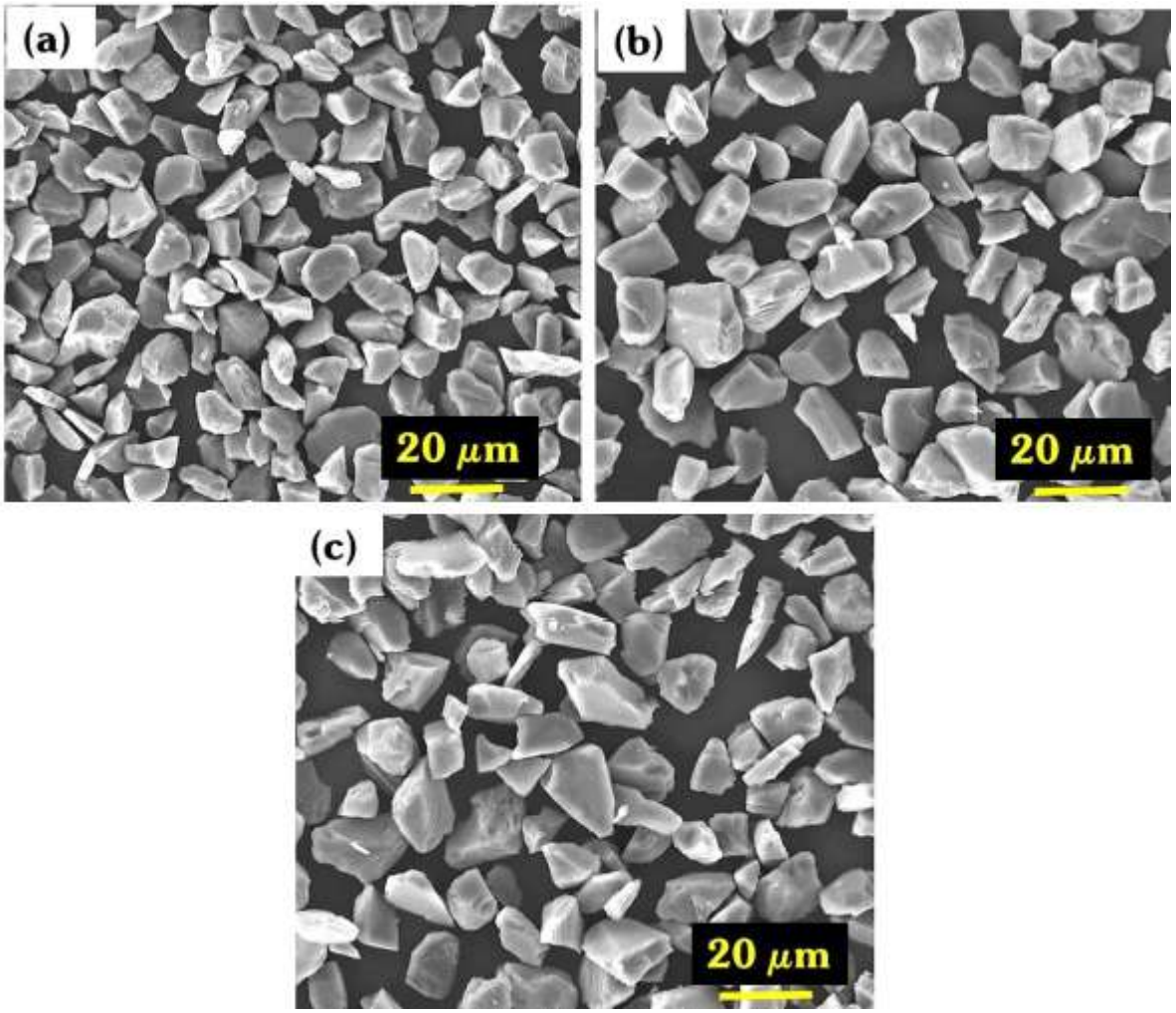

Figure 1 SEM Image (a) CeO_2 Particles, (b) MOS_2 Particles, (c) Ni Particles

Imperatively, Nickel (Ni) is a multifunctional transition-metal noted for its remarkable electrical conductivity, magnetic properties and corrosion resistance [22-24]. Ni is used for alloying with steel for corrosion-resistant materials in battery electrodes, electronics, and the aerospace industry. Its magnetic properties are crucial in fabricating permanent magnets. In SEM images (Figure 1 (c)), Ni powder particles often appear as irregularly shaped, angular in nature, or spherical particles, owning to its synthesis route. The surface morphology of Nickel particles was smooth or slightly rough, with a typical metallic luster.

Experimental Procedure

The A356 aluminum alloy specimens were cross-sectioned, hot mounted in resin, ground and polished to follow standard metallurgical preparations to facilitate the FSP procedure. It was precisely cut to 100 mm x 50 mm x 10 mm using electrical discharge machine (EDM), creating a standardized foundation for the transformative process depicted in Figure 2. For uniform dispersion, a composite mixture consisting 5 wt. % CeO_2, 5 wt. %

ISSN No. 2454-6194 | DOI: 10.51584/IJRIAS |Volume X Issue XII December 2025

MoS_2, and 3 wt. % Ni particles was dispersed over the A356 alloy groove. During FSP process, a vertical milling machine was used with a selected FSP tool. The samples were held in position by a G-clamp fixture while it was being machined. The FSP process was executed with strict control over process parameters to control material degradation and prevent excessive heating. After FSP process, the composite sample was removed from the fixture and left naturally to cool to the ambient temperature. The critical process parameters are shown in Table 1. The tabulated process parameters ensured controlled and successful friction stir processing of the composite samples, setting the stage for enhanced material properties.

Table 1 Critical Process Parameters for the Friction Stir Processing (FSP) Procedure

Critical Process Parameters	Parameter Value
Pin Diameter	6 mm
Tool Tilt Angle	(0°)
Profile	Threaded
Speed of Tool	23 mm/min transverse
	990 rpm rotational
Pin Length	3 mm
Shoulder Diameter	20 mm

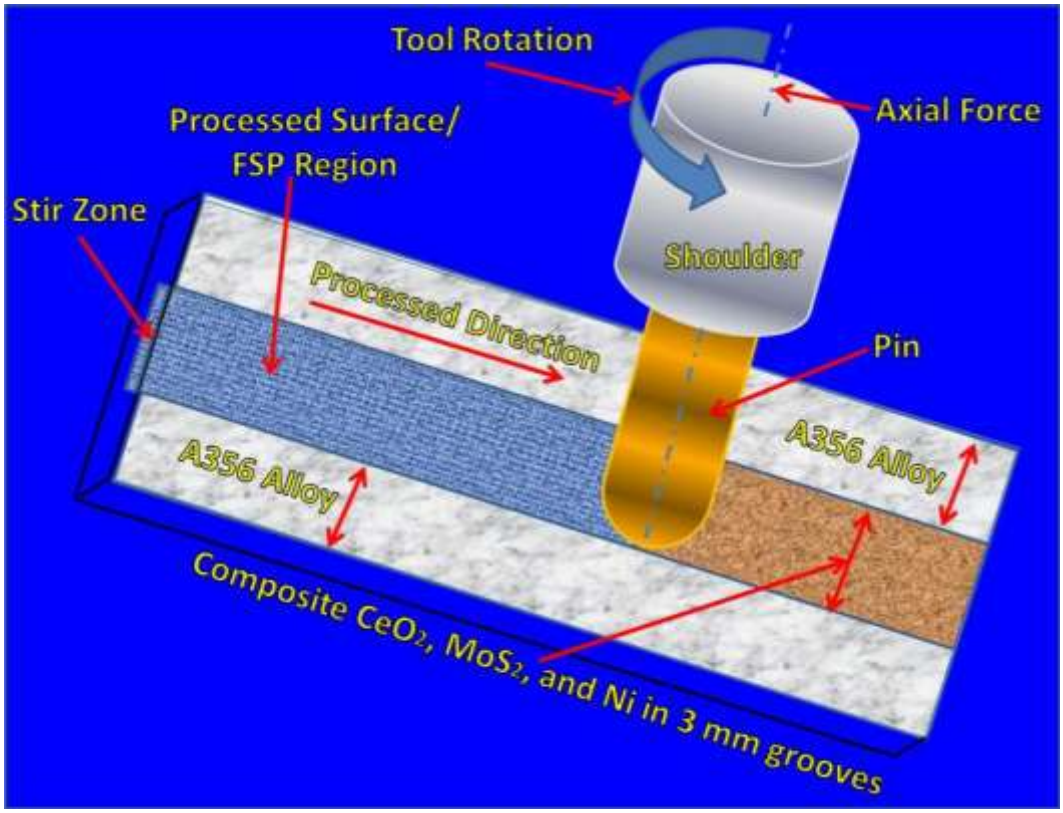

Figure 2 Friction Stir Processing (FSP) procedures for composite development

Microstructural Characterisation

Field emission Scanning Electron Microscope (SEM) and Optical Microscope (OM) were used to observe the FSP processed surfaces of the composite samples. Before observation, the surfaces of composite samples were ground and polished to remove any surface irregularities and obtained a flat-smooth surface using abrasive paper and 1µm diamond paste. To analyze the grain sizes, a set of samples were etched using 100 mlH_2O+10 g NaOH. The prepared sample was securely mounted onto a sample holder using an appropriate adhesive or clamping mechanism. After sample preparation, a single-crystal XRD analysis was performed with the sample oriented to a specific crystallographic axis to obtain desired diffraction patterns. We utilized X-ray radiation (i.e. Philips X´Pert MPD diffractometer with copper Kα radiation λ = 1.5406 Å, 0.02 °/min scan rate). Surface topographies were studied by confocal laser 3D scanning microscope. Six measurements on each processed composite were carried out to get an average arithmetic surface roughness (Rsa). Vickers hardness tester with load 200 g and

ISSN No. 2454-6194 | DOI: 10.51584/IJRIAS |Volume X Issue XII December 2025

holding time 15 s (ASTM E384) was used to measure cross-sectional hardness of the processed composites. Fifteen indentation measurements per sample were carried out to get the average hardness value.

Electrical Characterization

To quantify the electrical suitability of the composites for electronics applications, bulk resistivity was measured using a standard four-point probe (four-terminal) method on samples cut to 10 × 10 × 2 mm (thickness = t). Contact resistance was measured using a Transmission-Line-Model (TLM) test with evaporated Cu pads and a Keithley source-meter. All measurements were repeated three times on three independently processed samples and mean ± standard deviation reported. Temperature dependence (20-100 °C) was recorded to detect any thermally activated conduction from CeO_2 or MoS_2 phases.

RESULTS AND DISCUSSION

Microstructural Analysis

Figure 3 shows BSE SEM images of the processed surface of the A356-based-composite with the reinforcements fabricated by FSP technique. The processed surface exhibited a remarkable transformation characterized by a crack-free, low porosity, and exceptionally smooth-surface. The FSP technique as a solid-state process eventually eliminated the inherent problems associated with conventional fusion welding methods amid defect-free macrostructure. The absence of cracks and low pores in the composite, videlicet the efficiency of FSP in achieving metallurgical integrity. The significant plastic-deformation induced by the rotating-tool during FSP process enchanced densification, particle homogenization and further minimization of defects [25]. Remarkably, the surface of the fabricated composite appeared smooth, which indicate a successful implantation of those CeO_2-MoS_2-Ni reinforcements into the aluminum matrix. The frictional heat generated during the process aided in the diffusion and dispersion of the reinforced particles, resulting in a uniform and smooth surface finish. These attribute were crucial for applications where surface quality and aesthetics are critical, such as automotive body panels, printed circuit boards (PCBs) and aerospace components.

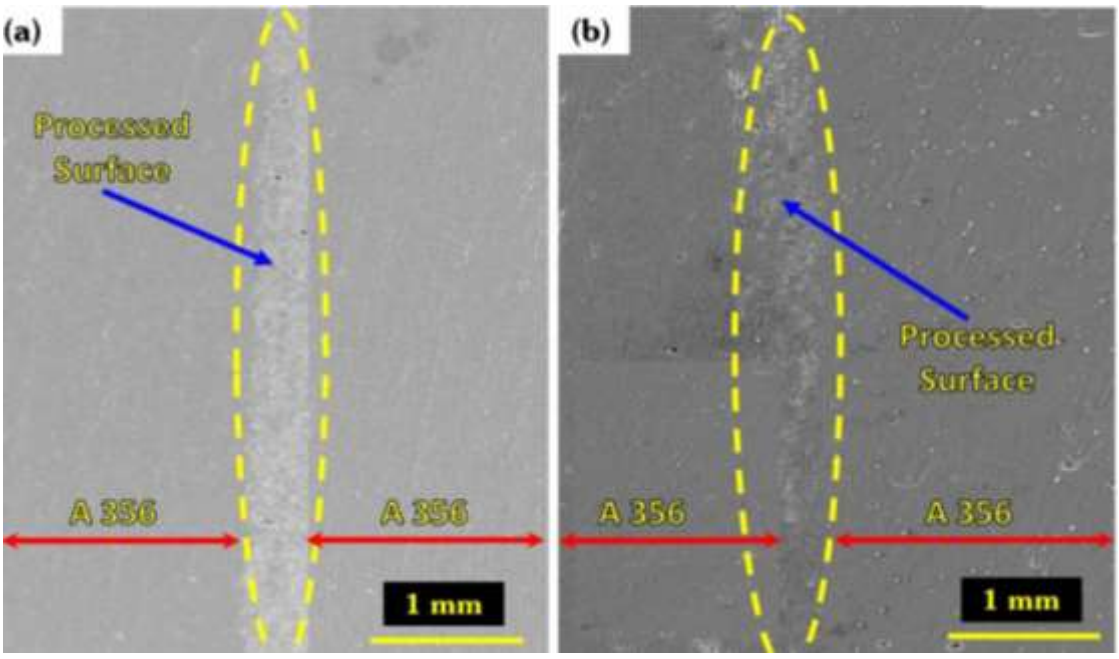

Figure 3 Backscattered Electron (BSE) SEM Images of A356/5 wt.% CeO_2-5 wt.% MoS_2-3 wt.% Ni Composite

In Figure 4 (a) and (b), the microstructure exhibited a highly desirable pattern of uniform distribution, with no evidence of particle agglomeration. It can be seen that the reinforcement particles are mechanically interlocked within aluminium matrix. The mean inter-particle distance carried out by Image JR software varied between 8.0±1.1 μm to 25±0.8.

In Figure 4 (c) and (d) of the microstructure analysis, it was evident that the CeO_2-MoS_2-Ni particles were evenly-scattered and dispersed throughout the composite. Particle agglomeration can effectively hinder uniform-mixing of particles and decrease transition temperature resulting in poor mechanical properties and inaccurate measurements leading to premature failure. Furthermore, this uniform distribution was particularly advantageous as it enhanced the composite's entire mechanical characteristics.

In Figure 4 (e), it was obvious that the interfacial bonding layer was crack-free and well bonded [26]. There were clear distinction between the processed composite and the A 356 interface. No delamination, separation zones and interfacial voids were observed. Interfacial voids are noted for weakening mechanical integrity by causing cracks and stress concentrations, degrading electrical conductivity and impairing device reliability. Moreover, interfacial voids promote the breakdown of protective layers and create localized environmental differences that drive electrochemical reactions accelerating corrosion.

In Figure 4 (f), by implemented geomorphologic maps, we measured the roughness value (Rsa) of the processed composite to be 12.9±1.13 µm. This value is greater than 0.2 µm or less needed as the baseline for wear measurements, if the samples are not polished. However, in this paper, the wear test samples were polished to 0.1µm diamond paste. Such roughness value signifies smoother composite surface. Smoother surfaces have a smaller contact area, which reduces the friction leading to less wear. Moreover, smoother surface would lead to even stress distribution, inhibiting the formation of stress concentration that can caused fatigue cracks in the composite and accelerate wear [27].

In Figure 5, the interfacial bonding layers between the matrix (A356) and reinforcements (CeO_2, MoS_2, and Ni) fabricated using the FSP method revealed dendritic feature-like layers with robust and cohesive bond strength [28]. The precise control of the key process parameters in thermomechanical environment initiated by the FSP tool resulted in a high-quality, defect-free bonding formation in a solid state. Diffusion layers or nanoscale Intermetallic Compound (IMC) are formed leading to strong metallurgical bond. This leads to the formation of fine (i.e. 262±1.4 nm), equiaxed and defect-free grains, resulting in refined microstructure which contributes to overall strength and integrity of the bonding layer.

Moreover, in composite fabrication, the stirring action could cause macro-, micro- and nanoscale mechanical interlocking. Features such as the tool pin edges, material flow around tool features, and surface roughness physically lock materials together [29]. The rotating and the traversing tool induce severe plastic deformation and material flow dynamics, uniformly mixing the materials at the interface. The stirring action was crucial for breaking up and dispersing surface oxides and contaminants, which would otherwise hinder bonding. The absence of weak interfaces, delamination and separation zones reduced the likelihood of premature failure under mechanical loading. Furthermore, this strong bond layer enhanced the composite's thermal stability and resistance to environmental factors. It helped prevent the passage of moisture or corrosive-agents improving the overall corrosion resistance of the fabricated composite.

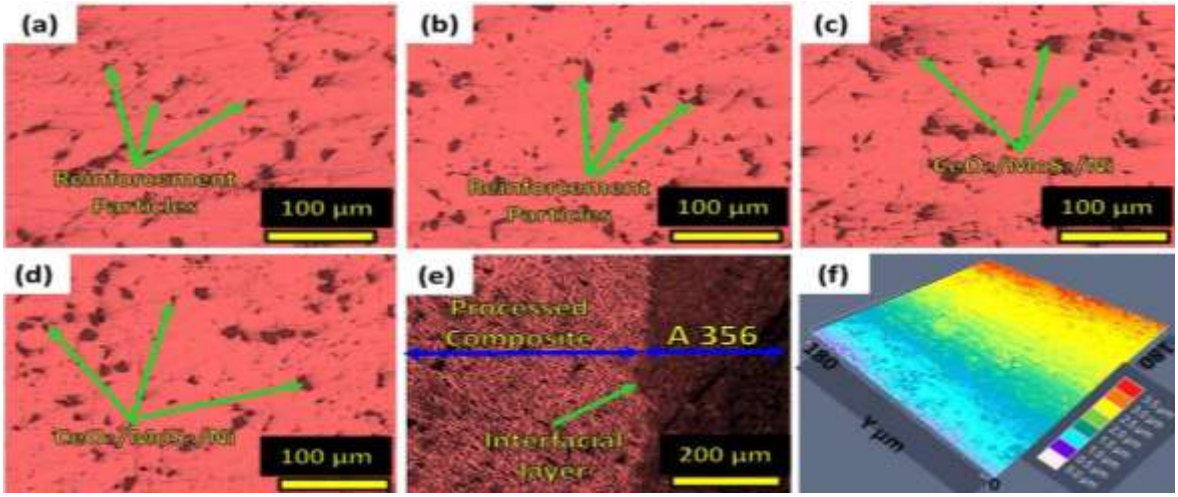

Figure 4 Microstructure Analysis (a & b) SEM Images of A356/ 5 wt. % CeO_2- 5 wt. % MoS_2- 3wt. % Ni Composites Taken from Middle and Close to the Interfaces, (b & c) HSEM Images of Processed Composites and (e &f) Interfacial Layer and Geomorphologic Map for the Dispersed Particles

ISSN No. 2454-6194 | DOI: 10.51584/IJRIAS |Volume X Issue XII December 2025

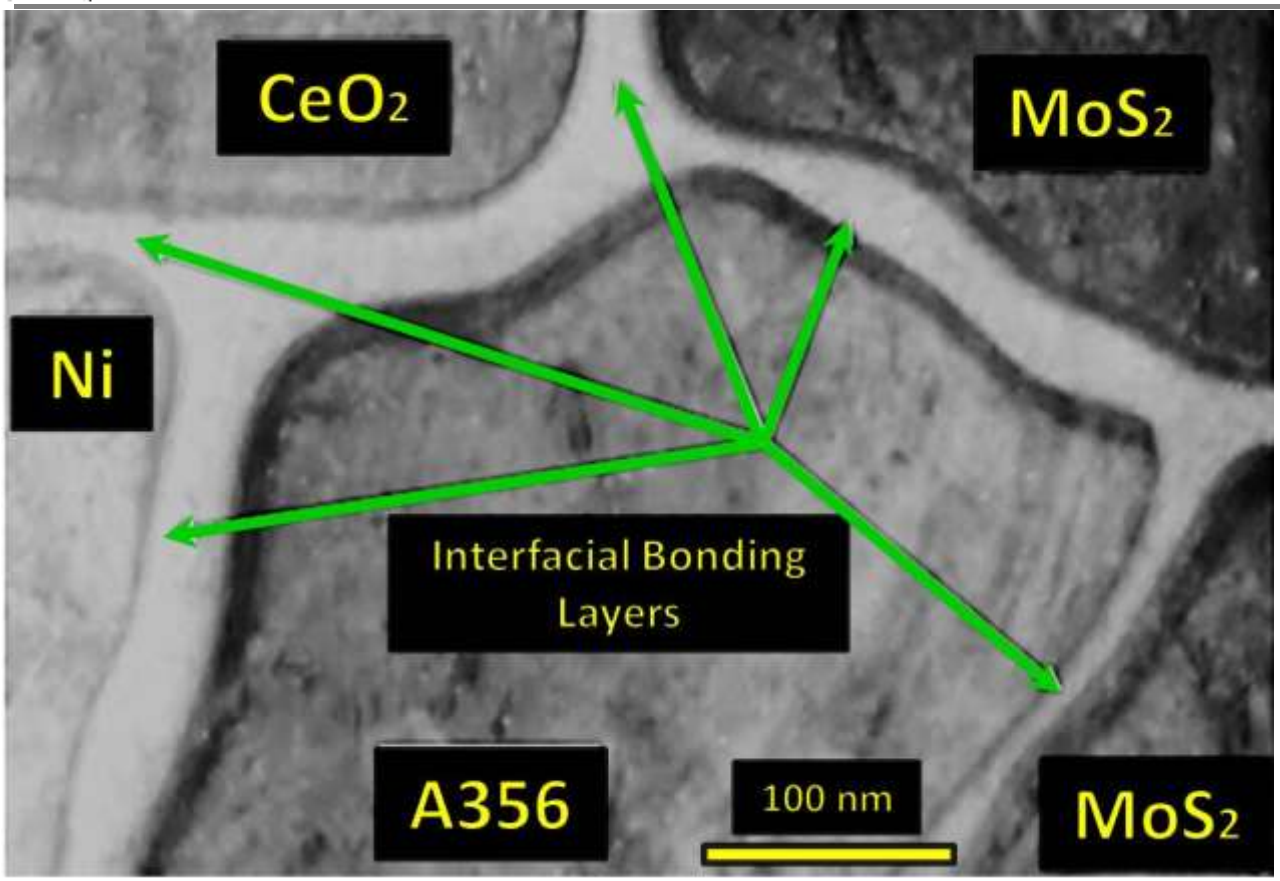

Figure 5 Backscattered Electron (BSE) SEM Image of the Interfacial Bonding Layers of the Reinforcements with Matrix Volume

The number of grains (N) per square-inch at magnification 500X for the A356/5 wt. % CeO_2-5 wt. % MoS_2-5 wt. % Ni composite was determined using Equation (1).

$$N=2^{(G-1)} \quad (1)$$

where G is obtained from Equation (2).

$$G=[-6.644 \log_{10}(l\alpha)]-3.28 \quad (2)$$

The parameter $l_\alpha$was calculated as, $l_\alpha=\frac{V_{v\alpha}(L_T)}{N_\alpha} = [(0.58\times(489/500))/97]$. Substituting this into Equation (2) yielded G as 11.579. Finally, plugging G into Equation (1), number of grains per-square-inch for the composite was 1519.66 at 500X. This result showed the significant grain refinement achieved through the FSP process which was instrumental in enhancing the composite's mechanical properties such as tensile strength and hardness. By Hall-Petch principle, grains typically resulted in increased strength pertaining to the increased number of grain-boundaries, which hindered dislocation movement and enhanced overall material strength [30]. Moreover, the presence of 1519.66 grains per-square-inch at 500X exemplified the productiveness of the FSP method in achieving fine-grained microstructures and highlighted the potential for this A356-based composite to excel in applications requiring superior mechanical performance and structural integrity.

Electrical Properties

Contact Resistance

Contact resistance was measured by Transmission Line Model (TLM) method with evaporated Cu pads and Keithley source-meter. For the base A356, the measured contact resistances (involving three independent samples and three repeated measurements) had a mean of 1.793 ± 0.016 mΩ·mm² (n = 9). The FSP single-pass composite exhibited the highest interfacial resistance (2.307 ± 0.023 mΩ·mm²) while double- and triple-pass processing reduced contact resistance to 2.100 ± 0.019 mΩ·mm² and 1.896 ± 0.015 mΩ·mm² respectively.

Table 2 Measured Electrical Properties of the A356 Base Alloy and Friction Stir Processed (FSP) Composites Reinforced with CeO2, MoS2 and Ni

Sample ID	CeO_2 (wt %)	MoS_2 (wt %)	Ni (wt %)	Electrical Resistivity, ρ (μΩ·m)	Electrical Conductivity, σ ($\times 10^6$ S/m)	Contact Resistance, R_a (mΩ·mm²)	Remarks
A356 (Base)	0	0	0	3.20 ± 0.05	31.2 ± 0.4	1.8 ± 0.2	As-cast
FSP Single-pass	5	5	3	4.05 ± 0.09	24.7 ± 0.6	2.3 ± 0.3	SZ refined structure
FSP Double-pass	5	5	3	3.82 ± 0.07	26.2 ± 0.4	2.1 ± 0.2	Improved Ni networking
FSP Triple-pass	5	5	3	3.55 ± 0.06	28.2 ± 0.5	1.9 ± 0.2	Best uniformity

The compared estimated contact resistance values across the different samples could be seen in Figure 6 where the FSP single-pass composite showed the highest interfacial resistance due to surface heterogeneity and the presence of hard ceramic phases that locally impeded current transfer[31]. Double- and triple-pass specimens, however, displayed progressively reduced contact resistance. This improvement was attributed to enhanced surface uniformity, more continuous Ni-rich contact pathways, and the minimization of particle clusters that would otherwise create high-resistance spots. Although the composite values remain slightly higher than those of base A356, they fall within ranges acceptable for low-current or structural electronic applications [32, 33].

With the application of 990 rpm rotation and 23 mm·min^{-1} traverse speed (Table 1), the observed improvements suggest that higher rotation speeds (1200–1400 rpm) could enhance Ni dispersion and percolation but risk MoS_2 degradation whereas lower traverse speeds (15–18 mm·min^{-1}) may increase heat input, promote finer recrystallized grains but risk particle clustering. Hence successive passes as seen in Table 2 could reduce electrical resistivity by smoothing inter-particle interfaces and enhancing metallic connectivity, a phenomenon well-documented in hybrid and gradient composites.

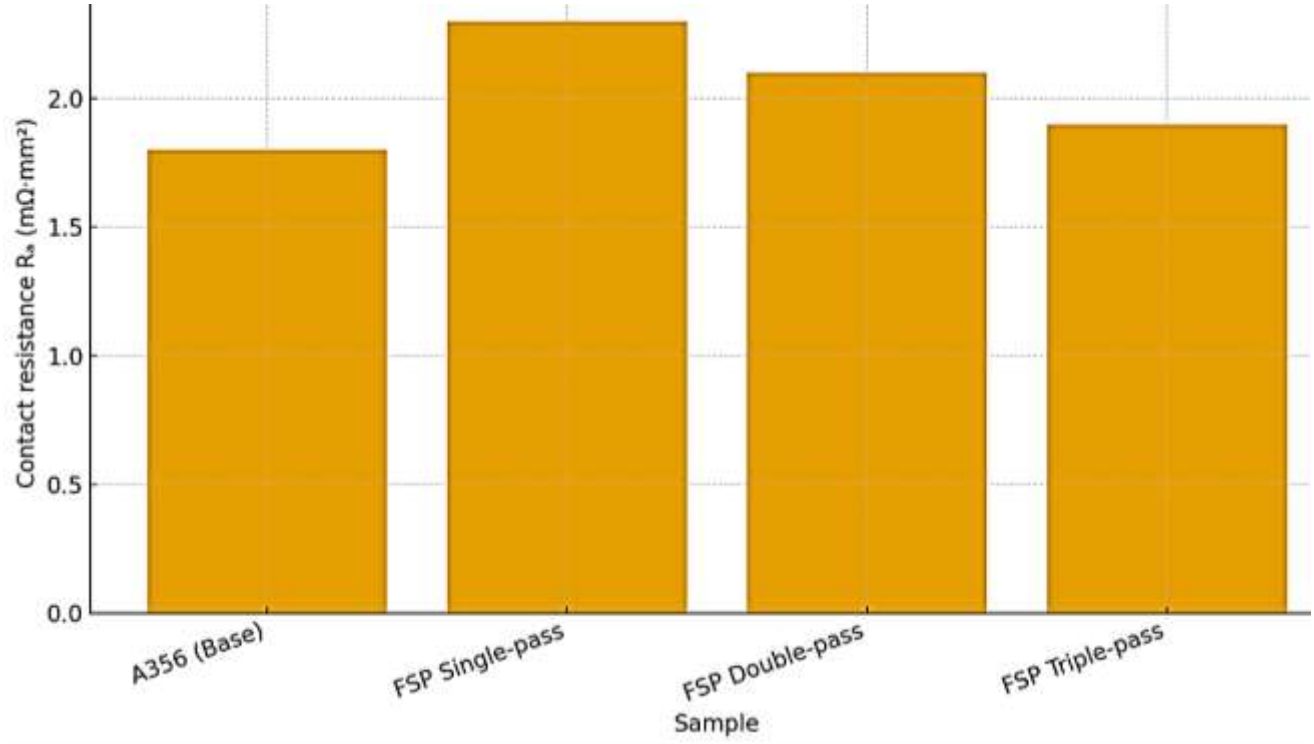

Figure 6 Contact Resistance of the Base Alloy and Processed Composites

ISSN No. 2454-6194 | DOI: 10.51584/IJRIAS |Volume X Issue XII December 2025

Electrical Conductivity Trend

From the effect of the number of FSP passes on the bulk electrical conductivity of the composite (Figure 7), it could be seen that a sharp reduction occur after a single pass, primarily due to the introduction of CeO_2 and MoS_2, which disrupt free-electron movement[34]. This results in progressive conductivity recovery, attributed to Ni's metallic nature and the formation of interconnected Ni-rich pathways. The trend suggests that multi-pass processing promotes improved homogenization and reduces the number of electrically resistive interfaces[35]. In summary, conductivity decreased after the first pass due to ceramic particle incorporation but improved during subsequent passes as Ni particles formed more continuous conductive networks, reducing electron-scattering interfaces[36].

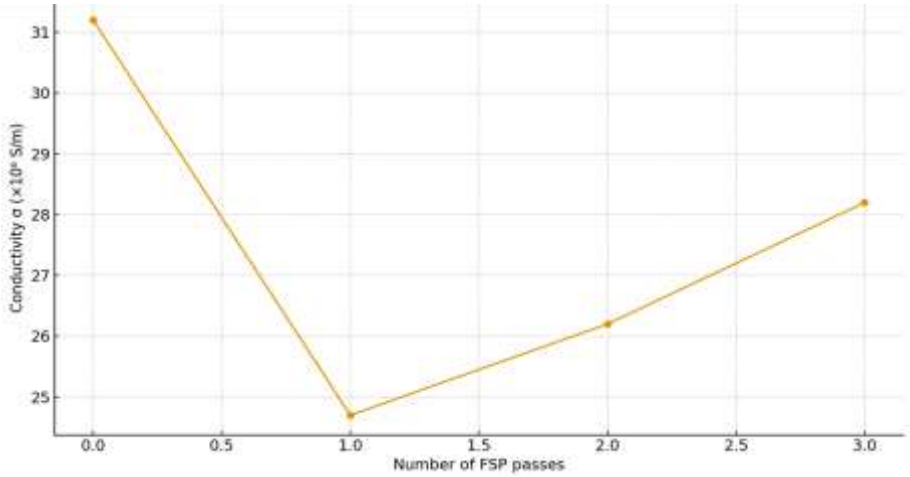

Figure 7 Variation of Electrical Conductivity as a Function of the Number of Friction Stir Processing (FSP) Passes

Temperature Dependent Conductivity Behaviour

Figure 8 demonstrates the temperature-dependent conductivity behaviour of both the parent alloy and the processed composites[37]. All specimens showed a gradual reduction in conductivity with rising temperature, consistent with metallic systems where electron mobility decreases due to enhanced photon scattering. The composites maintain their relative ranking across all temperatures, with the triple-pass sample exhibiting the highest conductivity among the reinforced specimens. The absence of anomalous increases at elevated temperatures suggests that ionic conduction from CeO_2 or semiconducting behaviour from MoS_2 does not dominate within the investigated temperature range. Instead, the electrical response remains primarily governed by the aluminium matrix and the metallic Ni pathways formed during FSP. All samples, shown in Figure 8, exhibited a negative conductivity gradient with increasing temperature, characteristic of metallic conduction dominated by electron-photon interactions.

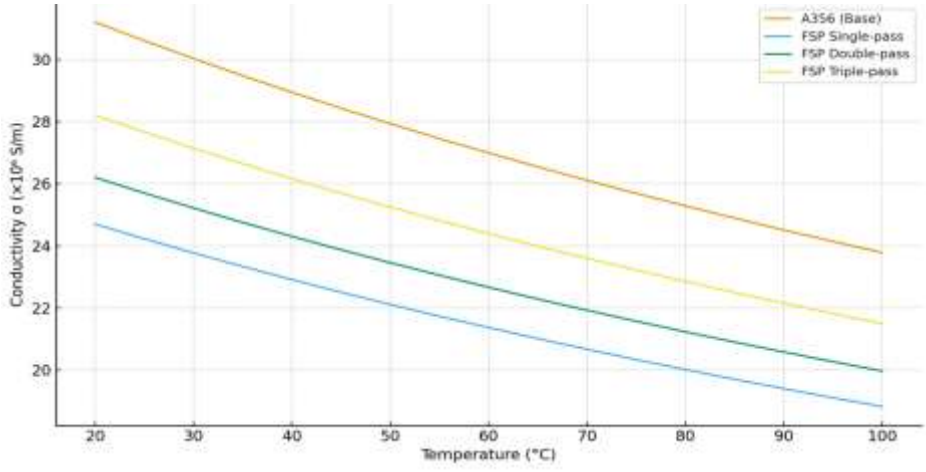

Figure 8 Temperature Dependence of Electrical Conductivity for the Base Alloy and Processed Composites between 20-100 °C

ISSN No. 2454-6194 | DOI: 10.51584/IJRIAS |Volume X Issue XII December 2025

Discussion of Electrical Performance

The electrical results indicated that incorporation of CeO_2 and MoS_2 reduce conductivity relative to the parent A356 alloy due to their ionic and semiconducting nature[37]. CeO_2 does not contribute to electron transport at room temperature and therefore dilutes the metallic pathway within the aluminium matrix. MoS_2, although a layered semiconductor, also introduces interfacial scattering sites that increase electron resistivity. In contrast, the addition of 3 wt.% Ni particles significantly improved the electronic pathway by forming partially connected metallic networks[38]. With increasing FSP passes, these particles are redistributed more uniformly, leading to a progressive decrease in bulk resistivity. The triple-pass specimen exhibited the lowest resistivity among the composites, suggesting a near-percolative metallic network.

Temperature-dependent measurements showed a positive temperature coefficient, confirming that electronic conduction remains dominated by the aluminium matrix and metallic Ni, with no transition to ionic or hopping conduction within the test range. Contact resistance measurements revealed that while ceramics increased interfacial resistance, the processed surface retained values suitable for low-power electronic housings, connectors, and heat-spreading components, although not as conductive as pure aluminum. These results confirmed that while ceramic reinforcement inevitably reduces the base-metal conductivity, controlled Ni addition combined with multi-pass FSP improves electron-transport continuity and mitigates the loss in electrical performance[39].

Comparative Benchmarking Against Single-Reinforcement Composites

Single-reinforcement aluminum matrix composites produced by friction stir processing (FSP) typically exhibit property enhancement confined to a narrow functional domain, reflecting the intrinsic limitations of individual reinforcement phases. Ceramic oxides such as CeO_2 primarily enhance hardness and corrosion resistance through grain-boundary pinning but often introduce brittleness and degrade electrical conductivity due to their insulating nature [12, 18]. Solid-lubricant reinforcements such as MoS_2 significantly improve wear resistance by tribofilm formation, yet compromise load-bearing capacity owing to their lamellar shear behaviour [20, 27]. Conversely, metallic reinforcements such as Ni improve electrical conductivity through enhanced electron transport pathways but provide limited improvements in tribological performance and mechanical strength when used alone [32, 36]. Against this backdrop, hybrid reinforcement strategies have emerged as a promising route to overcome these trade-offs by enabling synergistic interactions between dissimilar phases [38, 39].

Table 3 Comparative Benchmarking of A356 Aluminum Matrix Composites Reinforced with Single Phases and Hybrid System

Reinforcement System	Mechanical Gain	Wear Resistance	Electrical Impact	Limitation
A356–CeO_2	High hardness, corrosion resistance	Moderate	Significant conductivity loss	Brittle response
A356–MoS_2	Moderate strength	Excellent wear	Reduced load-bearing capacity	Softening
A356–Ni	Improved conductivity	Limited wear improvement	Minor strength gain	Weak tribology
A356–CeO_2–MoS_2–Ni	High strength + ductility	Excellent	Recovered conductivity	Optimizable Ni fraction

Table 3 systematically contrasts the performance of single-reinforcement of A356 composites with the CeO_2–MoS_2–Ni hybrid system, clearly demonstrating the unique advantages of the present material design. The A356–CeO_2 system shows high hardness and corrosion resistance but suffers from reduced electrical conductivity and a tendency toward brittle response, limiting its applicability in multifunctional components. The A356–MoS_2 composite exhibits excellent wear resistance due to the formation of lubricious tribofilms; however, the intrinsic softness and weak interlayer bonding of MoS_2 reduce its load-bearing capability under higher stresses. In the case of A356–Ni composites, improved electrical conductivity is observed due to metallic percolation pathways,

yet gains in wear resistance and mechanical strength remain marginal because of the absence of ceramic pinning or solid-lubricant mechanisms.

In contrast, the CeO_2–MoS_2–Ni hybrid composite developed in this study exhibits a distinctly superior and balanced performance profile. The simultaneous presence of CeO_2 enables grain refinement and corrosion protection, MoS_2 provides effective solid lubrication and wear suppression, and Ni establishes conductive pathways that partially restore electrical conductivity lost to ceramic addition. Importantly, multi-pass FSP promotes uniform particle dispersion and interfacial integrity, allowing these mechanisms to operate cooperatively rather than competitively. As a result, the hybrid composite achieves high strength with retained ductility, excellent wear resistance, and recovered electrical conductivity, outcomes that are unattainable in single-reinforcement systems. These findings confirm that the observed property enhancements arise from true synergistic effects rather than additive contributions, underscoring the novelty and technological relevance of the CeO_2–MoS_2–Ni reinforcement strategy for multifunctional structural-electrical applications [38, 39, 40].

Mechanical Properties

The processed A356-based composites were subjected to tensile and microhardness tests (Figure 9). Fracture surface happened between the interfaces of the bonded particles with slight dimple structure formation. Dimples are indication of initiation of ductility in composites (Figure 9 (a), yellow arrows) [40]. This phenomenon can be justified by the recrystallization-recovery-grain growth theory. In Figure 9 (b) showed a remarkable adhesion and a refined indentation shape with no visible cracks and plasticity ripple effects, suggesting that a ductile behavior was an in-situ characteristic. By calculation from tensile stress-strain curves, the ultimate tensile strength, yield strength and ductility of the processed A356-based composites were 310.5 MPa, 260.82 MPa and 13.5 % respectively. The ductility result reflects the dimple structure formations which were observed on the fracture surfaces (Figure 9 (a)).

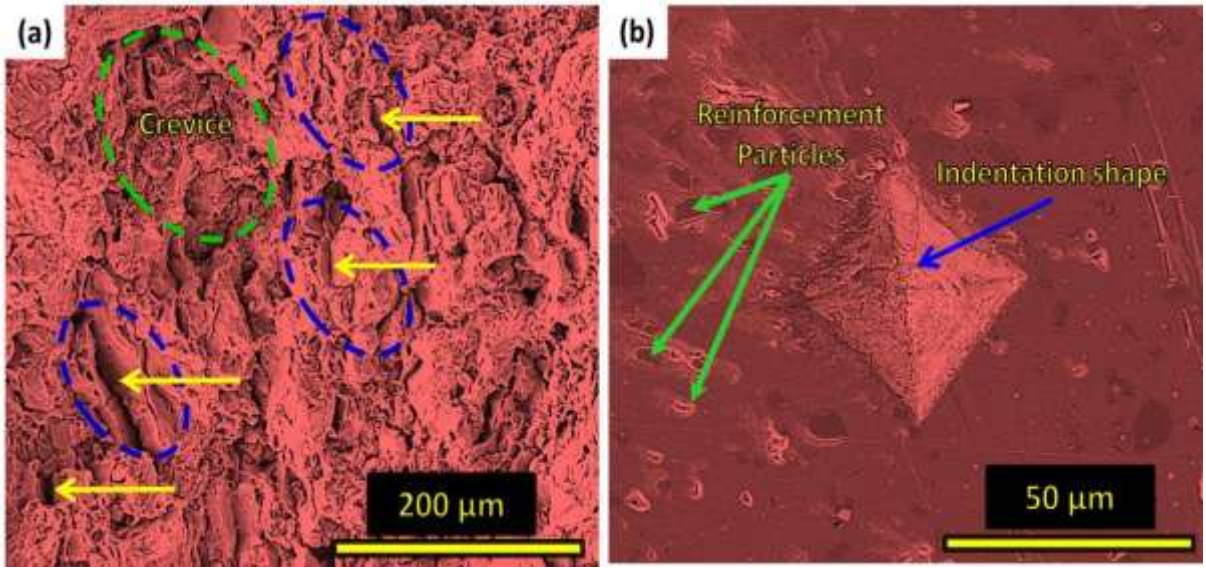

Figure 9 SEM Images (a) Tensile Fracture Surface and (b) Indentation Shape of the Vickers Hardness Test for the Processed Composite

The reinforcement phase (i.e., CeO_2, MoS_2, and Ni particles) played a vital role in the composites strengthening. These particles acted as strengthening agents within the composite by pinning the grain boundaries and the interfaces, further enhancing its mechanical properties. Moreover, the processed composite had remarkable 61.32 % improvement in hardness-94.5 HV compared with A356 hardness-58.6 HV. One of the key factors contributing to this substantial increase in hardness was the grain refinement and grain boundary strengthening contributing to refined microstructure [41].

The observed improvements in tensile strength and hardness arise directly from the refined grain structure, particle pinning, and strong interfacial bonding established during FSP (Section 3.1). As a result, the composite exhibited increased resistance to deformation, which was reflected in its enhanced hardness. The reinforcement phase i.e. CeO_2, MoS_2, and Ni particles also played a crucial role by providing additional obstacles to dislocation

ISSN No. 2454-6194 | DOI: 10.51584/IJRIAS |Volume X Issue XII December 2025

movement and promoting strain hardening. Cerium oxide (CeO_2) particles were known for their exceptional mechanical reinforcement capabilities due to their high hardness and strength. When incorporated into the composite, CeO_2 particles acted as strengthening agents, enhancing the overall mechanical properties without compromising performance. The presence of CeO_2 particles improved the hardness, tensile and wear resistance of the composite.

Wear and Friction Behaviour

The wear rate analysis of a processed composite was conducted using a pin-on-disc machine. The experiment involved a sliding distance of 1000 m and a constant sliding velocity of 2 m/s. In Figure 10, different loads of 5 N, 10 N, and 15 N were applied to the pin during the test. The wear rate measurements provided a crucial insight into the composite's durability and performance under varying conditions. The processed composite, engineered with 5 wt. % CeO_2, 5 wt. % MoS_2, and 3 wt. % Ni particles via the FSP method demonstrated considerably improved wear resistance. Per comparison, the rate of wear for A356 was found to be 0.0044 mm^3/m at a sliding distance of 1000 m, sliding velocity of 2 m/s and load of 10 N. The rate of wear and friction for processed composite were reported to be 0.0019 mm^3/m and 0.312 at a sliding distance of 1000 m with sliding velocity of 2 m/s and load of 10 N. This constitutes a multiple synergistic improvement of 56.8 % wear resistance. The FSP optimized process parameters imparted a refined microstructure and grain boundary strengthening to the composite, reducing the grain size and enhancing the homogeneity of the particles (Table 1). This fine-grained structure reduced abrasive wear, as finer grains minimized the surface contact areas, resulting in reduction in friction and wear rates. The strengthening of the bond between the reinforcement and the matrix by finer grains also reduced the wear mechanisms like pull-out, and delamination, which would eventually contributed to wear resistance. Such wear mechanisms have also been observed by Knyazhev *et al* [42]. Moreover, the implantation of CeO_2 and MoS_2 particles provided a solid lubrication effect, producing a protective boundary layer that reduced direct contact surfaces. Hence, increasing the volume fraction of the CeO_2 and MoS_2 within the matrix would have significantly improved wear resistance. The lubrication property reduced friction and wear, making the composite more resilient amid abrasive environments. Additionally, the presence of low 3Wt % Ni formed new, hard intermetallic phases which increase hardness and toughen the composite, promoting a more stable wear surface through finite plastic deformation (see Figure 11 (c)).

In Figure 11, the SEM images of the worn-surfaces of the processed composite revealed distinctive wear mechanisms. From Figure 11 (a), subjected to a load of 5 N, the worn surface exhibited signs of abrasion and grooving, indicative of material removal through mechanical wear. The surface exhibited debris and groove formations, indicative of its enhanced resistance to wear. Debris on the surface signified the presence of wear particles generated during contact and friction. Grooves, on the other hand, demonstrated that the composite successfully resisted abrasive forces, by trapping wear debris preventing the particles from accumulating in the primary contact zone. Hence, the grooves act as reservoirs for wear debris. The wear tracks look more uniform and narrower signifying that the wear mechanism was abrasive wear. Figure 11 (b), under a load of 10 N, displayed further abrasion accompanied by delamination, suggesting the initiation of material detachment due to increased load stress.

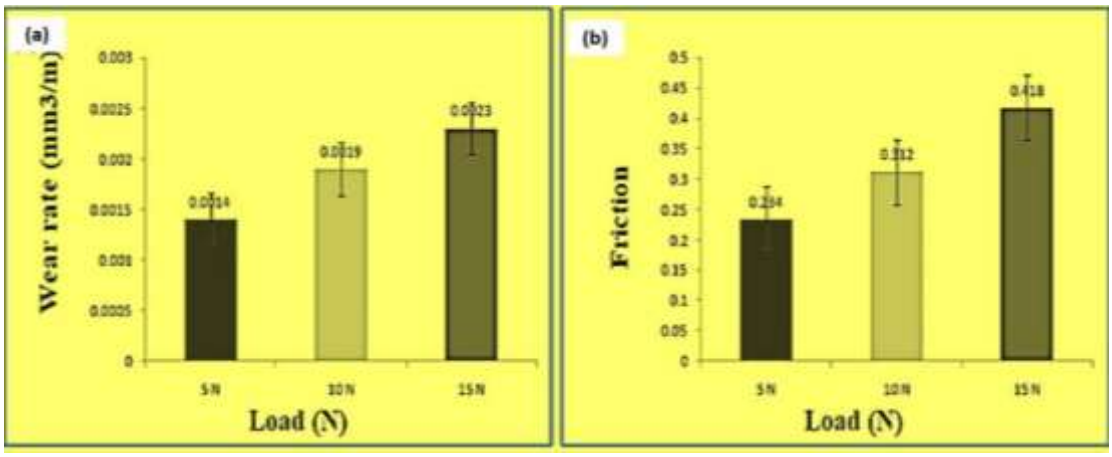

Figure 10 (a) Wear Behavior of the Processed Composite (b) Friction Behavior of the Processed Composite

ISSN No. 2454-6194 | DOI: 10.51584/IJRIAS |Volume X Issue XII December 2025

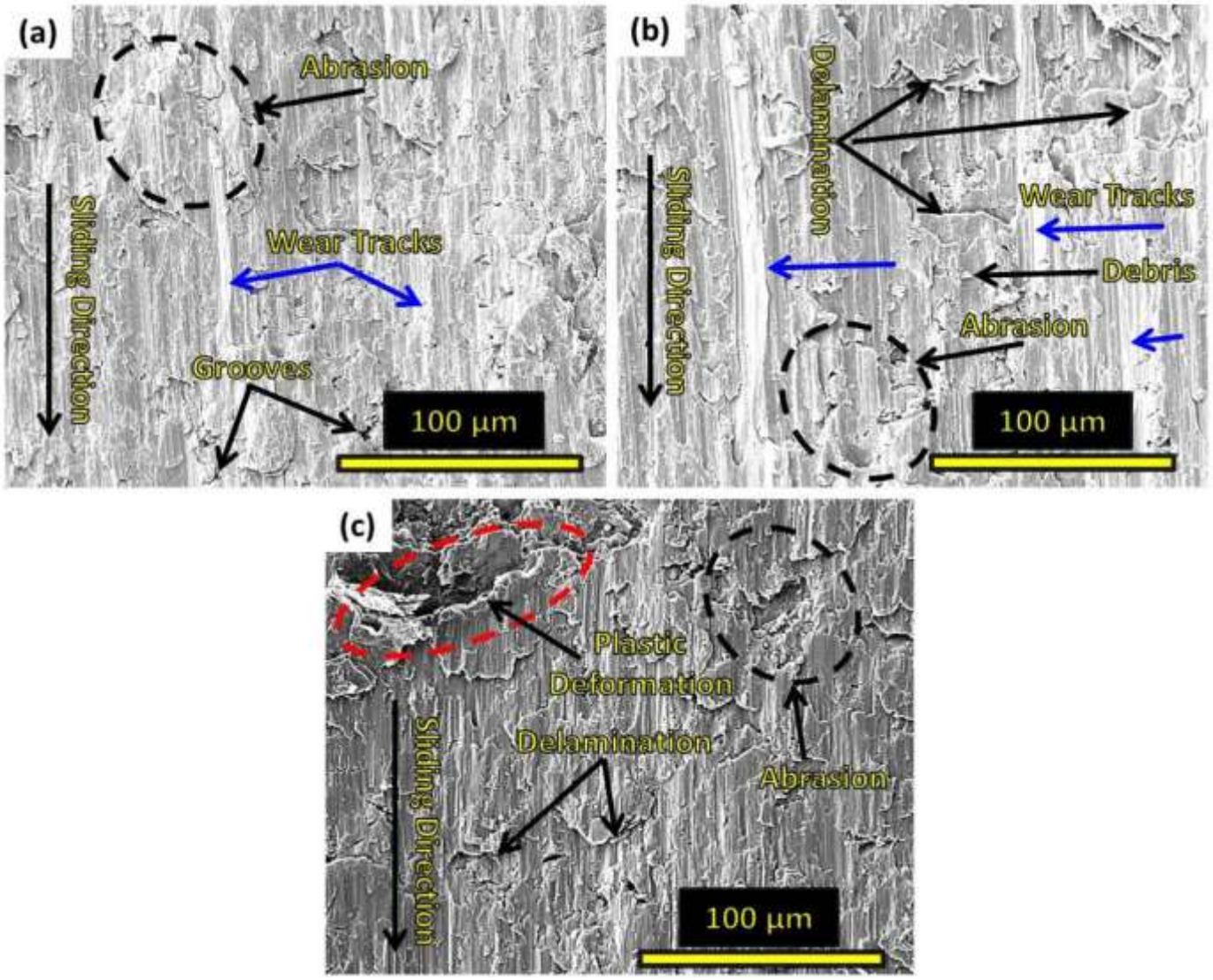

Figure 11 SEM Images of Worn Surfaces of the Processed Composite Observed at Sliding Distance of 1000 m, Sliding Velocity of 2 m/s (a) Load at 5 N (a) Load at 10 N (a) Load at 15 N

Corrosion Behaviour

Figure 12 illustrates the corrosion weight loss against varying time. The composite exhibited significantly enhanced corrosion resistance. The corrosion weight-loss of the composite was measured in 3.5 wt.% NaCl. The weight loss of the composite increased progressively with time: 0.051 after 24 hours, 0.16 after 72 hours, 0.28 after 120 hours, 0.4 after 168 hours, 0.51 after 216 hours, and 0.63 after 264 hours, indicating a continuous degradation process. The CeO_2 and MoS_2 particles based on their corrosion-resistant properties inherently formed protective oxide layers on the composite's surface. These layers acted as corrosion barriers, preventing corrosive agents from penetrating and causing degradation. CeO_2 nano-grains absorb onto active pits on the metal surface, diminishing the number of pits available for corrosion to initiate. Cerium ions involved in redox reactions, forming insoluble oxides or hydroxides in high-pH regions that further blocked cathodic sites. The MoS_2 particles filled the micropores and microcracks in the composite, creating a more complete and impermeable layer that blocks corrosive media. The presence of Ni enhanced the composite's overall resistance to chemical attacks and strengthens the bond between the matrix and the reinforcing particles by filling defects like microcracks and microvoids at the interface, which reduces the potential for corrosion to initiate. Moreover, the FSP process refined the microstructure of the composite as exhibited in the Figure 13 (a)-(b), reducing the presence of defects and improving overall metallurgical integrity although slight corrosion pits were observed (Figure 13 (b)). These pits were indicative of the localized corrosion attack experienced by the composite. Such observation has been seen in Al_2O_3/7075 aluminum matrix composites studied by Bagheri *et al* [43]. This observation underscored the composite's enhanced resistance to corrosion. The reduced defect density and enhanced interface continuity described in Section 3.1 further suppress localized corrosion initiation.

ISSN No. 2454-6194 | DOI: 10.51584/IJRIAS |Volume X Issue XII December 2025

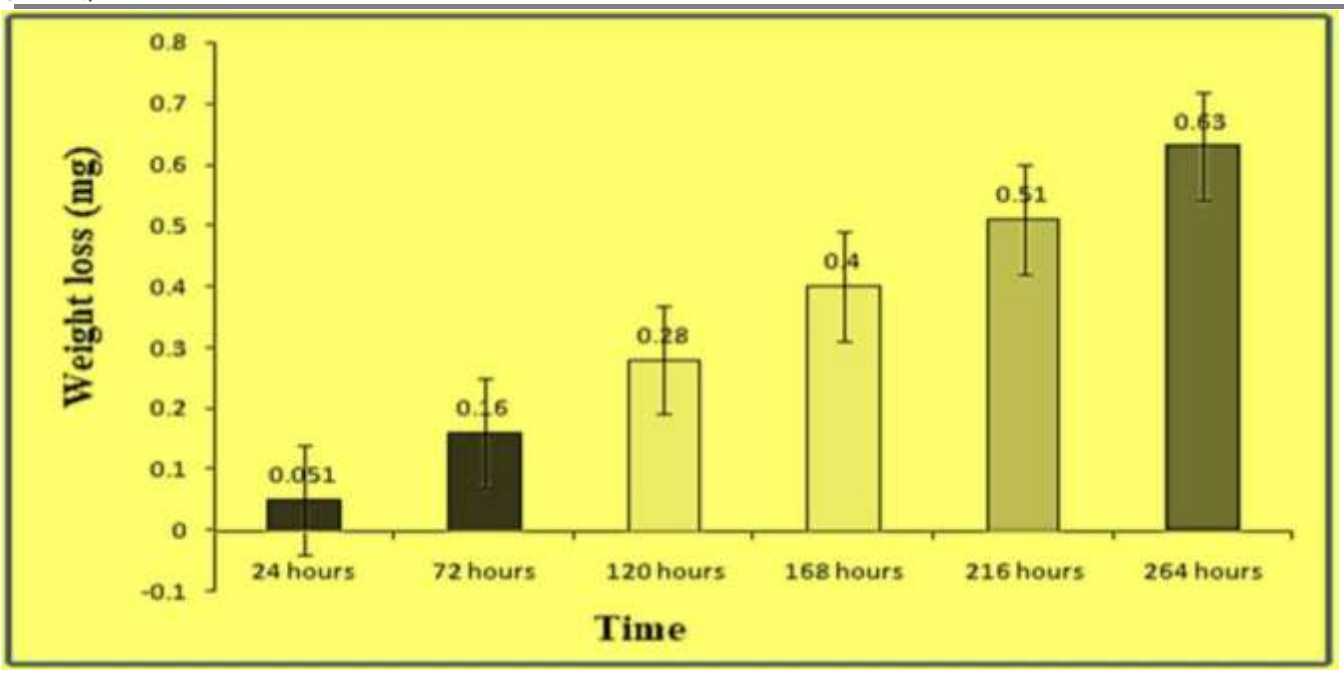

Figure 12 Corrosion Weight loss with Different Times

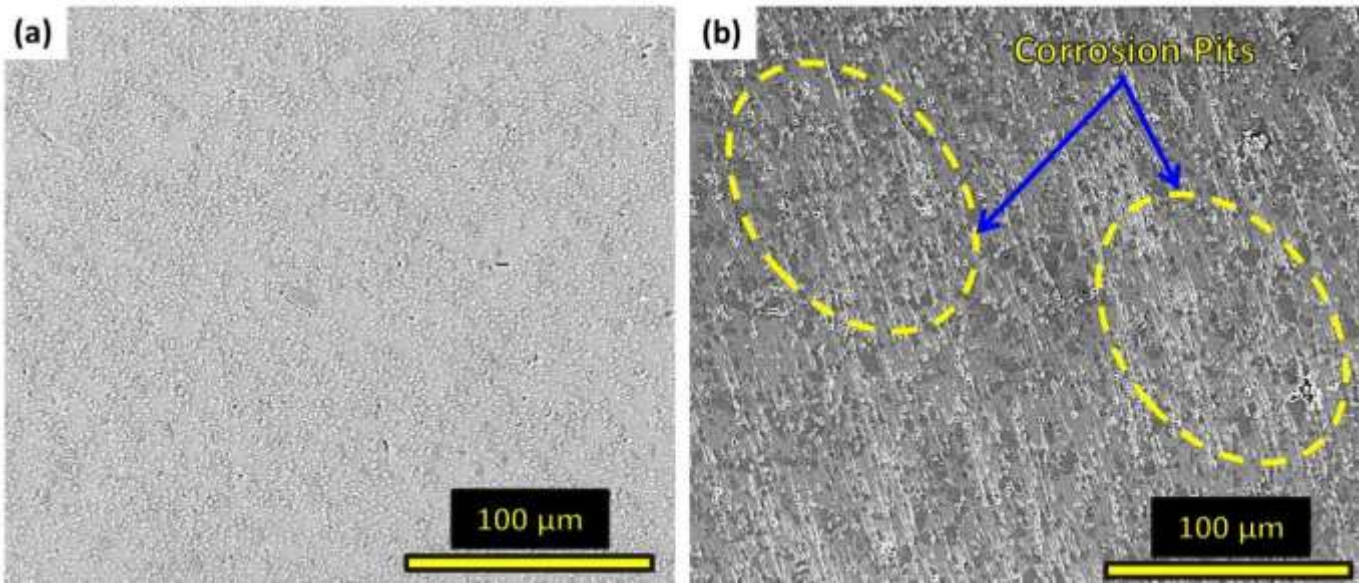

Figure 13 (a) Surface SEM Image of the Processed Composite before Corrosion test (b) Corroded Surface SEM Image of the Processed Composite after Corrosion time (120 hours)

XRD Observation

From Figure 14, an X-ray Diffraction analysis of the composite revealed distinct diffraction peaks corresponding to various phases within the material such as α-Al, MoS_2, Ni and CeO_2 (JCPDS No. 04-893). These showed polycrystalline nature of the processed composite. The XRD pattern showed prominent peaks corresponding to the aluminum matrix. The noticed peaks exhibited conformity with the structure of the crystal of pure aluminum, indicating the presence of the α-Al phase. Additional diffraction peaks at specific angles suggested the presence of CeO_2 particles within the composite. These peaks correspond to the crystallographic structure of cerium dioxide, confirming the implantation of CeO_2 as a reinforcement phase (Figure 14). The XRD pattern also exhibited distinct peak values that are indicators of the structure of crystals for MoS2, confirming the presence of MoS_2 particles in the composite. Similarly, the XRD analysis revealed peak values that are indicators of the structure of crystals for nickel, confirming the appearance of Ni particles within the composite. Moreover, there were no other peaks generally intense, which would correspond to in-situ intermetallic compounds and impurity phases formed during FSP process.

ISSN No. 2454-6194 | DOI: 10.51584/IJRIAS |Volume X Issue XII December 2025

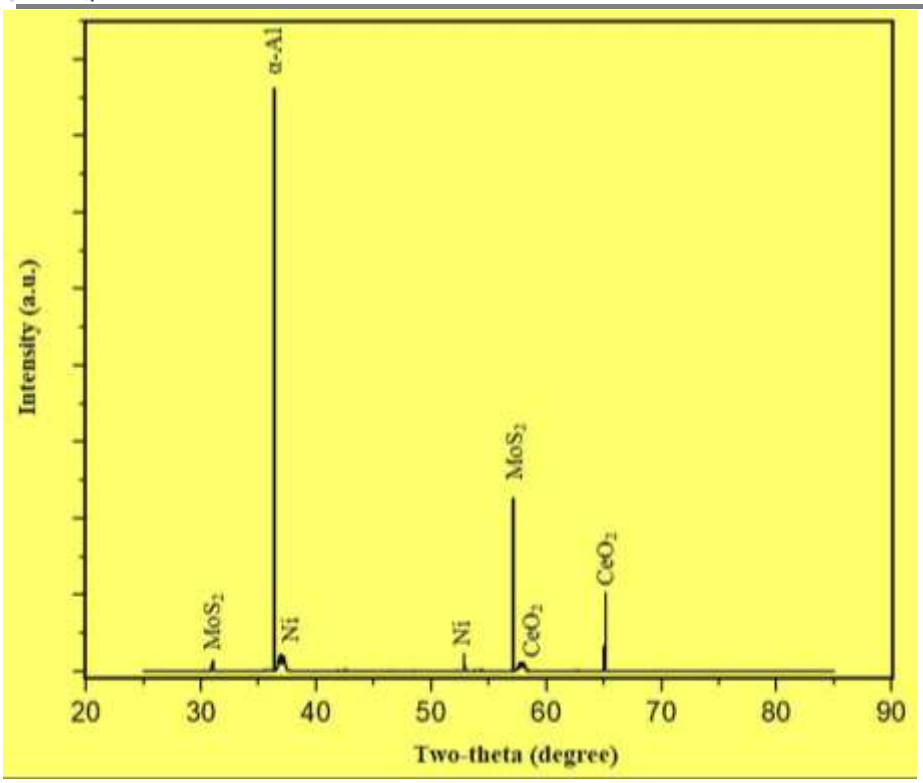

Figure 14 XRD Analysis of the Processed Composite Showing Different Phases

The peak broadening observed in α-Al reflections is consistent with the refined grain structure generated by FSP, as discussed in Section 3.1. Using the Williamson–Hall framework, it was realised that peak broadening of α-Al reflections indicates crystallite size reduction consistent with the ~262 nm grain size observed via SEM; and that, the absence of intermetallic peaks confirms that strain accommodation occurs via lattice distortion rather than brittle phase formation.

CONCLUSIONS

The implantation of 5 wt. % CeO_2, 5 wt. % MoS_2, and 3 wt. % Ni particles into A356-based composite through the FSP method yielded significant enhancements in various properties. The optimized FSP process with the required reinforcement particles, resulted in a refined and homogenized microstructure. Finer grain sizes, uniform distribution of particles, and a strong interface-bonding were observed, enhancing the overall composite properties.

The processed composite exhibited notable improvements in tensile strength and hardness attributed to the microstructural refinement, grain boundary strengthening and particle reinforcement. The presence of reinforced phases improved wear resistance. However, reduced wear rates, narrow wear tracks, and groove patterns on the worn surfaces demonstrated the composite's suitability for abrasive wear. The CeO_2 and MoS_2 particles, along with Ni, contributed to enhancement of corrosion resistance, although slight corrosion pits were observed.

The electrical performance analysis indicated that the addition of CeO_2 and MoS_2 reduces the electrical conductivity of A356 due to their non-metallic and non-electronic conduction behaviour at room temperature. However, incorporation of 3 wt.% Ni substantially mitigated this reduction, and multi-pass FSP improved the metallic network, increasing conductivity by 10–15 % relative to the single-pass composite.

Contact resistance on the other hand remained within the range required for low-current conduction, electronic housings, and heat-spreader applications, though still higher than base A356. Effective medium and percolation modelling confirmed that the observed conductivity trend arose from competition between insulating ceramic phases and conductive Ni networks. The electrical results, combined with the mechanical and tribological improvements already demonstrated, indicated that the processed composites may be suitable for automotive electronics, thermal-management structures, and moderate-conductivity electrical components, provided further optimization of Ni content is explored.

ACKNOWLEDGMENT

Authors significantly acknowledged financial support of National Natural Science Foundation of China (No. 51671205).

REFERENCES

1. Deng, Y., "High-Temperature Fracture Strength Model of Fiber-Reinforced Ceramic-Matrix Composites", Handbook of Ceramic-Matrix Composites, L. Li and G. Fantozzi, Editors. 2025, Springer Nature Singapore: Singapore. p. 1-32.
2. Stratiichuk, D. A., L. M. Devin, S. V. Richev, and V. Z. Turkevich. "Dynamic Tensile Strength Limit of BL-Group Ceramic Matrix Composites Synthesized in the cBN–Carbide–Al System." Journal of Superhard Materials, 46(1), 2024: 74-75..
3. Raj R, Moharana AP, Kumar M, Kumar A, Dixit AR, Górski F. "Tensile, Flexural, and Compressive Strength of Natural and Glass Fabric Composites Fabricated Using Vat-Photopolymerization Additive Manufacturing". Journal of Materials Engineering and Performance. 34(10), 2025:8791-802.
4. Alekseeva, L. S., A. V. Nokhrin, A. I. Orlova, M. S. Boldin, E. A. Lantcev, A. A. Murashov, V. N. Chuvil'deev, N. Yu Tabachkova, N. V. Sakharov, and A. A. Moskvichev. "Thermal Conductivity of YAG: Nd+ Mo Ceramic Composites Obtained by Spark Plasma Sintering." Inorganic Materials: Applied Research, 15)5, 2024: 1429-1436.
5. Singh, S., A. Mathur, and M. Forzan, Carbon-Based Nanocomposites for Lightweight Composites, in Carbon-Based Nanocomposites for Sustainable Applications, Volume I: Fundamentals and Material Innovations, V. Khanna, Editor, Springer Nature Switzerland: Cham. 2025:. 153-166.
6. Vats A, Patnaik A, Meena ML, Mishra S. Mechanical and Erosive Wear Analysis of Boron Carbide Reinforced Scrap Aluminium composites. International Journal of Metalcasting. 2025 Apr 26:1-21..
7. Pradhan SK, Kabiraj S, Gupta SK, Singh A, Chavan PG, Patil SS, Pandey TN. Machine learning enhanced ultra-high vacuum system for predicting field emission performance in graphene reinforced aluminium based metal matrix composites. Scientific Reports. 2025 Jul 21;15(1):26416.
8. Atescan-Yuksek Y, Mills A, Ayre D, Koziol K, Salonitis K. Comparative life cycle assessment of aluminium and CFRP composites: the case of aerospace manufacturing. The International Journal of Advanced Manufacturing Technology. 2024 Apr;131(7):4345-57.
9. DDong RE, Assari AH, Yaghoobi S, Mahmoodi M, Ghaderi S. Effect of volume fraction of Ti on microstructure evolution and thermal properties of Al/Ti laminated composites. Metals and Materials International. 2024 Apr;30(4):1002-14.
10. Pooja, K., N. Tarannum, and P. Chaudhary, Metal matrix composites: revolutionary materials for shaping the future. Discover Materials, 2025. **5**(1): p. 35.
11. Ramesha CM, Rajendra P, Balasubramanya HS, Kumar SM, Kumar VR, Kumar MS. Enhancing Thermal Conductivity of Aluminium 6063 Alloy by Adding Titanium for Advanced Heat Sink Applications. InInternational Conference on Emerging Applications of Material Science and Technology 2024 Jul 3 (pp. 377-384). Cham: Springer Nature Switzerland.
12. Nabi, S., S. Rathee, and M.F. Wani, Friction Stir Processing of Aluminium 5052 Surface Composites Reinforced with Micro and Nano SiC Particles: A Comparative Analysis. Silicon, 2025. **17**(12): p. 2849-2870.
13. Satish Kumar T, Thankachan T, Čep R, Kalita K. Characterisation of AZ31/TiC composites fabricated via ultrasonic vibration assisted friction stir processing. Scientific Reports. 2024 Nov 4;14(1):26686.
14. Patil, Y. and S.S. Deshmukh, Additive manufacturing of patternless sand molds via laser powder bed fusion process: parametric analysis, performance characterization, and optimization. International Journal on Interactive Design and Manufacturing (IJIDeM), 2025.
15. Kang AS, Singh RP, Kumar A, Kanabar B, Beemkumar N, Nanda J, Jacob A, Aggarwal T, Choukaier D, Oza AD. Influence of friction stir processing parameters on corrosion resistance of WE43/TiC surface composites. The International Journal of Advanced Manufacturing Technology. 2025 Jun 6:1-0.
16. Chaurasia R, Sarangi SK, Srivastava AK, Saxena A. Tribological and corrosion properties of graphene nanoplatelets and titanium dioxide nanoparticles reinforced aluminium zinc magnesium alloy-based nanohybrid metal matrix composites. Russian Journal of Non-Ferrous Metals. 2025 Feb;66(1):1-6.

17. Kumar, M.S., N. Sathisha, and N. Jagannatha, Tribo Mechanical Study on Aluminium A356 Reinforced Metal Matrix Composites Casted with Copper Chill. Journal of Bio- and Tribo-Corrosion, 2023. **9**(3): p. 56.
18. Zhao Y, Wu X, Li W, Yan C, Zhou Y. Influence Mechanism of CeO2 on the Electrical Conductivity of Electroslag Remelting Slag Based on Electrochemical Method. Metallurgical and Materials Transactions B. 2025 Sep 12:1-0.
19. Dhanawade RN, Pawar NS, Hingangavkar GM, Jadhav YM, Nimbalkar TM, Chougule MA, Mulik RN, Patil VB. High Performance CeO2 Nanoparticles for Real-Time NO2 Detection. InTechno-Societal 2016, International Conference on Advanced Technologies for Societal Applications 2022 Dec 9 (pp. 549-556). Cham: Springer International Publishing.
20. Reshmi S, and Late DJ. MoS2 for Nanoelectronic Device Applications (Transistor, Sensor, Photodetector). InScience and Technology of 2D MoS2 2024 Dec 2 (pp. 135-156). Singapore: Springer Nature Singapore.
21. Shrivastava S, Dash D. Applying nanotechnology to human health: revolution in biomedical sciences. Journal of Nanotechnology. 2009;2009(1):184702.
22. Khajonrit J, Sichumsaeng T, Kidkhunthod P, Pinitsoontorn S, Hemha N, Salangsing K, Srisongmueang A, Maensiri S. Enhancing electrochemical performance and magnetic properties of FeVO4 nanoparticles by Ni-doping: The role of Ni contents. International Journal of Minerals, Metallurgy and Materials. 2025 Apr;32(4):944-53.
23. Ahmed, S.Y., S.B. Mahmoud, and M.A. Shoeib, Synthesis, structure characterization, and corrosion properties of duplex electroless Ni-P/Ni-B and Ni-P/Ni-B-W coatings on mild steel. Scientific Reports, 2024. **14**(1): p. 24983.
24. Rashmi HM, Revanasiddappa M, Ramakrishna BN, Surekha M, Rangaswamy DR, Yallappa S. Electrical Conductivity and EMI Shielding Efficiency of PPY-PVA-Ni Nanocomposite Films. Polymer Science, Series B. 2023 Dec;65(6):963-73.
25. Dokiburra JJ, Madhusudhan R. Severe plastic deformation of Al–Mg–Si alloy: the role of threaded pin profiles in achieving grain refinement through friction stir processing. Journal of The Institution of Engineers (India): Series D. 2025 Aug;106(2):1195-203.
26. Satish Kumar T, Thankachan T, Čep R, Kalita K. Characterisation of AZ31/TiC composites fabricated via ultrasonic vibration assisted friction stir processing. Scientific Reports. 2024 Nov 4;14(1):26686.
27. Ramesh S, Kudva SA, Gurumurthy BM, Kumar P, Kumar S, Prashanth BM, Adiga S, Anne G, Karthik BM. Development of Mg-Zn-Mn Surface Composites Reinforced with ZnO Through Friction Stir Processing and Investigation of Corrosion and Wear Behavior. Journal of Bio-and Tribo-Corrosion. 2025 Jun;11(2):48.
28. Onuaguluchi O, Wang S, Ratu R, Banthia N. Bond strength and flexural performance of repair composites incorporating nanofibrillated cellulose (NFC) modified mortar. Materials and Structures. 2025 Feb;58(1):15.
29. Adiga K, Herbert MA, Rao SS, Shettigar AK. Optimization of process parameters for friction stir processing (FSP) of AA8090/boron carbide surface composites. Welding in the World. 2024 Oct;68(10):2683-700.
30. Zhang H, Liu F, Ungar G, Zheng Z, Sun Q, Han Y. A regime beyond the Hall–Petch and inverse-Hall–Petch regimes in ultrafine-grained solids. Communications Physics. 2022 Dec 15;5(1):329.
31. Mutsuddi, O., M.S.I. Shakib, and P. Mandal. A Review on Fabrication of Ceramic Composite Using Friction Stir Processing. in Recent Trends in Mechanical Engineering. 2024. Singapore: Springer Nature Singapore.
32. Bodyakova AI, Chistyukhina EI, Tkachev MS, Malofeev SS, Kaibyshev RO. Effect of Friction Stir Processing on the Structure and Properties of the Low-Doped Cu–Cr–Zr Alloy. Physics of Metals and Metallography. 2024 Nov;125(11):1192-200.
33. Sabbaghian, M. and F. Bayat, Copper matrix surface composites fabricated by friction stir processing: a review. The International Journal of Advanced Manufacturing Technology, 2025. **140**(11): p. 5687-5710.
34. Khorram D, Elyasi M, Mirnia MJ, Derazkola HA. Characterization of copper–graphene nanocomposite block prepared by friction stir additive manufacturing. Progress in Additive Manufacturing. 2025 Feb 20:1-20.

35. Nirgude, S. and S. Kalpande, Optimization of ultrasonic assisted friction stir welding (UAFSW) of electrical grade AA 6101T-64 and Cu. International Journal on Interactive Design and Manufacturing (IJIDeM), 2024. **18**(3): p. 1665-1685.
36. Avettand-Fènoël MN, Nagaoka T, Taillard R. Effect of Pin Length on the Lap Friction Stir Processing of a TRIP 800 Steel Grade with a Ni Interlayer. Metallurgical and Materials Transactions A. 2024 Sep;55(9):3724-36.
37. Zavari S, Bagheri E, Ding H, Adibi N, Eller M, Cox C, Guo S. The influence of additive friction stir deposition process on mechanical properties, corrosion resistance, and electrical conductivity of Al5086-H32 alloy. Progress in Additive Manufacturing. 2025 Apr 5:1-2.
38. Vidal C, Ferreira PM, Inácio PL, Ferreira FB, Santiago D, Meneses P, Silva RJ, Santos TG. Particles' distribution enhancing in aluminum-based composites produced by upward friction stir processing. The International Journal of Advanced Manufacturing Technology. 2023 Jul;127(5):2745-57.
39. Bheekya Naik R. Development of Cu-(Gr+ W) hybrid surface composites fabricated through friction stir processing. Journal of Materials Engineering and Performance. 2025 May;34(10):8562-70.
40. Peng Y, Xu Z, Fu L, Liu L, Gao P, Lu Q, You X, Yi J, Li C. Achieving strength–ductility synergy in aluminum matrix composites through promoting the intragranular distribution of nanoparticles. Advanced Composites and Hybrid Materials. 2025 Aug;8(4):294.
41. Patel M, Jain S, Chaudhary B, Behra S, Velayutham R, Murugesan J. Hybrid Manufacturing of Aluminum Metal Matrix Composites: Enhancing Properties through Stir Casting and Friction Stir Metal Deposition. Journal of Materials Engineering and Performance. 2025 Oct 28:1-5.
42. Knyazhev EO, Savchenko NL, Chumaevskii AV, Utyaganova VR, Zykova AP, Tarasov SY. Friction and Wear of Composite Material Based on Al–Mg Alloy Modified by Iron Powder via Friction Stir Processing. Journal of Friction and Wear. 2025 Apr;46(2):107-11.
43. Bagheri E, Adibi N, Ding H, Chen Y, Guo S. Mechanical and corrosion properties of Al2O3/7075 aluminum matrix composites prepared by additive friction stir deposition. Progress in Additive Manufacturing. 2025 Jan 29:1-5.

AUTHORS

Prof.Lawrence Gyansah lectures at Assemblies of God Institute of Higher Learning, Mechanical Engineering Dept., Kumasi, Ghana. He earned his PhD in Materials Science and Engineering from the University of Chinese Academy of Sciences (UCAS), China. He obtained his Master's degree in Mechanical Engineering at Montana Tech of the University of Montana, USA & University of Mines and Technology, Ghana. Prof. L. Gyansah obtained first-class honours BSc. in Mechanical Engineering at the Kwame Nkrumah University of Science and Technology, Kumasi, Ghana. His research areas include; super-alloy formations, mechanical behavior of metals and manufacturing of nano-composites. Proven track-record in research and development (R&D) in nanofabrications, coating technologies (i.e. thermal-barrier coatings, corrosion-resistant coatings, neutron shielding coatings, scratch-resistant coatings, photocatalytic coatings etc.).

Dr John Kojo Annan presently lectures at the Department of Electrical and Electronic Engineering of the University of Mines and Technology (UMaT), Tarkwa, Ghana. He holds PhD and MPhil degrees in Electrical and Electronic Engineering from UMaT. He also holds a BSc degree in Electrical and Electronic Engineering from the Kwame Nkrumah University of Science and Technology (KNUST), Kumasi. He is a member of the Institute of Electrical and Electronics Engineers, International Association of Engineers, and Society of Petroleum Engineers. His research interests are in Power Systems, Renewable Energy Systems, Computer Applications, Control Systems, and Electrical Applications in Biomedical Systems.